PAPER

Check for updates

Synthesis of hollow core–shell ZnFe$_2$O$_4$@C nanospheres with excellent microwave absorption properties

Huimin Hao, [ID] Liming Wang,* Lihui Xu, Hong Pan, Liuqi Cao and Kouqin Chen

The special hollow core–shell structure and excellent dielectric-magnetic loss synergy of composite materials are two crucial factors that have an important influence on the microwave absorption properties. In this study, hollow ZnFe$_2$O$_4$ nanospheres were successfully synthesized by a solvothermal precipitation method firstly; based on this, a C shell precursor phenolic resin was coated on the ZnFe$_2$O$_4$ hollow nanospheres' surface by an *in situ* oxidative polymerization method, and then ZnFe$_2$O$_4$@C was obtained by high-temperature calcination. Samples were characterized by SEM, TEM, XRD, XPS, BET, VSM, VNA. The results show that the maximum reflection loss (RL$_{max}$) reaches −50.97 dB at 8.0 GHz, and the effective bandwidth (EAB) of hollow core–shell structure ZnFe$_2$O$_4$@C is 3.2 GHz (6.16–9.36 GHz) with a coating thickness of 3.5 mm. This work provides a useful method for the design of lightweight and high-efficiency microwave absorbers.

1. Introduction

With the booming development and wide application of electrical equipment, especially the coming of age of 5G, electrical interference and electromagnetic radiation have caused serious electromagnetic pollution problems, which not only interfere and damage the precision of electronic equipment but also do great damage to human health and safety.[1–3] Microwave absorbers play a great role in solving these issues, as they can dissipate electromagnetic energy and convert it into heat or other forms of energy to be consumed. Ferrite, as a kind of material with stable chemical properties, a simple preparation process, low price, and high impedance matching, has attracted extensive attention in the field of microwave absorption materials. Among them, spinel ZnFe$_2$O$_4$ is particularly prominent in the field of microwave absorbers due to its chemical stability and superparamagnetism.[4–7] Examples include ZnFe$_2$O$_4$ nanospheres, ZnFe$_2$O$_4$ nanorods, and ZnFe$_2$O$_4$ nanoparticles.[4,8,9] However, the single ZnFe$_2$O$_4$ only has excellent magnetic loss and relatively weak dielectric loss performance, and this single complex permeability makes the impedance matching imbalanced; at the same time, as a ferromagnetic material, ZnFe$_2$O$_4$ has a large density, these two problems make ZnFe$_2$O$_4$ unable to meet the requirements of high-quality microwave absorbing materials, such as lightweight, wide frequency band and thin thickness.[8] Based on the above problems, it is necessary to improve microwave absorption performance of ZnFe$_2$O$_4$ by composite modification.

As a kind of dielectric material, carbon material has a wide range of applications in the field of microwave absorbers, such as carbon fiber,[10] graphene,[11] carbon nanosphere,[12] carbon nanotubes,[13] *etc.* Wang *et al.*[14] designed multi-shell hollow carbon spheres through hydrothermal method combined with calcination, etching means, and obtained an excellent microwave absorption material that exhibits the RL$_{max}$ of −48.5 dB and a wide effective microwave absorption bandwidth. Carbon material with good dielectric loss can be combined with ferromagnetic material to construct a binary composite of a nanosphere with outstanding microwave absorption performance. Many researchers have demonstrated that this scheme is feasible to improve microwave absorption performance. Deng[15] synthesized FeCoNiZn alloy@carbon nanocomposite with a unique heterostructure, which owned the RL$_{max}$ of −54.46 dB at 16.65 GHz and the effective bandwidth reaches 4.19 GHz under the thickness of 1.62 mm. Gu[16] prepared Fe$_3$O$_4$/HPC (hierarchical porous carbon) by a facile strategy. Fe$_3$O$_4$/HPC composite presented a significant improvement of the microwave absorption compared with a single HPC frame when the Fe$_3$O$_4$ filling content is 40%, the RL$_{max}$ value is up to −57.8 dB at 7.36 GHz with a thinner thickness of 3.48 mm, and the bandwidth lower than −10 dB ranging from 11.92 GHz to 17.92 GHz.

It's worth noting that not only do the components of the composite have an impact on the microwave absorption performance, its structure is also a fatal factor. In general, a regular structure may put an excellent influence on the microwave absorption of composite, which is evidenced by many studies, such as yolk–shell structure,[17] multi-shell structure,[18] hollow structure,[19] and so on.[20] The hollow structure can not only reduce the weight of the sample, which is beneficial to

School of Textiles and Fashion, Shanghai University of Engineering Science, Shanghai 201620, China. E-mail: wlm@sues.edu.cn; Tel: +86-13601982260

the preparation of lightweight microwave absorbing materials, but also conducive to the multiple reflection and scattering of electromagnetic waves because of the huge cavity inside the hollow sphere, which promotes to achieve the effect of attenuation of electromagnetic waves.

Based on the preparation of hollow $ZnFe_2O_4$, we introduce dielectric C material to prepare $ZnFe_2O_4$@C composite with a core–shell structure. On one hand, the introduction of a C shell increases the interfacial area of the sample, which is conducive to the generation of interfacial polarization. At the same time, a large amount of free charge accumulates on the interface, which is beneficial to the formation of dipole polarization. The synergistic effect of dielectric loss and magnetic loss enhance the impedance matching degree of the sample, so the electromagnetic wave can enter the material to the maximum extent for subsequent attenuation. A core–shell or hollow structure can reduce the density of the material and increase the specific surface area of the material. Wang[21] construct Co_7Fe_3@C composite with core–shell structure, which with an ultra-thin coating thickness of 1.6 mm, and the RL_{max} is −117.4 dB at 11.9 GHz. At the same time, the composite has the most excellent effective microwave absorption bandwidth and is as wide as 9.2 GHz, during the range 8.8–18 GHz. This result proves the core–shell structure composite should be a promising high-efficiency microwave absorber.

In this paper, we prepared a hollow core–shell $ZnFe_2O_4$@C nanosphere by self-assembly and subsequently calcined it at high temperatures. The obtained sample owns a special structure that meets the requirements of lightweight and high strength of excellent microwave absorbing materials. In specific, the sample presents excellent microwave absorption performance with the RL_{max} is −50.97 dB, and the effective bandwidth reaches 3.2 GHz (6.16–9.36 GHz) under the thickness of 3.5 mm. It is no doubt that the obtained composite will have a widespread application in the field of microwave absorption during the next few years.

2. Experimental section

2.1 Materials

Iron chloride ($FeCl_3 \cdot 6H_2O$), zinc chloride ($ZnCl_2$), urea, ethylene glycol, polyethylene glycol 2000 (PEG-2000), resorcinol, formaldehyde solution (38%), ammonia solution (38%), ethanol absolute (99.5%). All reagents were pure analytical grade without further purification.

2.2 Synthesis of hollow $ZnFe_2O_4$ nanospheres

The hollow structure $ZnFe_2O_4$ nanospheres were prepared by thermal precipitation. Firstly, 0.45 g $ZnCl_2$, 1.784 g $FeCl_3 \cdot 6H_2O$ were dissolved into 60 ml ethylene glycol and magnetically stirred for 2 hours to obtain a homogeneous solution. After that, 2 g precipitant urea and 2 g PEG-2000 were added, and then magnetically stirred until the solution hybrid completely, then transferred into a 100 ml Teflon lined jar in an autoclave and heated at 200 °C for 24 h. At high temperatures, $Zn(OH)_2$ is decomposed into ZnO and Fe_2O_3 first and then forms small

$ZnFe_2O_4$ particles. With the assistance of PEG-2000, small $ZnFe_2O_4$ particles are arranged to form hollow $ZnFe_2O_4$ nanospheres. This phenomenon can be attributed to Ostwald's ripening theory. Finally, samples were separated by magnetic separation technology, washed with water and alcohol until the washing solution was clarified, and then dried overnight in an oven at 60 °C for 12 h to obtain hollow $ZnFe_2O_4$ nanospheres in the form of black powder.

2.3 Synthesis of core–shell hollow $ZnFe_2O_4$@C nanospheres

0.18 g of obtained hollow $ZnFe_2O_4$ nanospheres were dispersed in a mixture solution of 18 ml distilled water, 36 ml absolute ethanol, and 0.84 ml concentrated ammonia solution by mechanical agitation. Next, 0.2 g of resorcinol and 0.16 ml of formaldehyde were respectively added, and the mixture solution was continuously mechanical stirred for polymerization at 30 °C for 2 h, forming a layer of phenolic resin (PR) on the surface of hollow $ZnFe_2O_4$. After polymerization, the obtained hollow $ZnFe_2O_4$@PR nanospheres were obtained by magnetic separated and washed with water and ethanol absolute and dried at 60 °C for 12 h under vacuum. Subsequently, the as-prepared $ZnFe_2O_4$@C precursor ($ZnFe_2O_4$@PR) nanospheres were calcined under N_2 atmosphere at 650 °C for 2 h with a heating rate of 5 °C min^{-1} to obtain the hollow core–shell $ZnFe_2O_4$@C precursor nanospheres.

2.4 Characterization

The crystal type and crystallinity of the samples were analyzed by X-ray powder diffraction (XRD) with the scanning angle was 10°–80° and the scanning rate was 10° min^{-1}. The types and valence states of each element in the sample were measured by a Thermo Scientific K-Alpha+ X-ray photoelectron spectrometer (XPS), which was equipped with a monochromatized AlKα X-ray source ($h\nu = 1486.6$ eV). The Raman spectrum was determined by a Raman spectrometer (Raman) using an Ar ion laser with a wavelength of 514 nm as the excitation source for spectroscopic measurements. The surface morphology and internal structure of the samples were characterized by scanning electron microscopy (SEM) and transmission electron microscopy (TEM), respectively. Nitrogen adsorption and desorption isotherms of samples were collected by a fully automatic specific surface and porosity analyzer. Samples were degassed at 200 °C under vacuum for 2 h before measurements, and then the specific surface area and pore size distribution of samples were determined by Brunauer–Emmett–Teller (BET) method and Barrett–Joyner–Halenda (BJH) model, respectively. The vibrating sample magnetometer (VSM) was used to perform the hysteresis loop of the sample, and the saturation magnetization (M_s) and coercivity (H_c) of the sample were obtained by data analysis. In order to record the reflection loss of electromagnetic waves and the corresponding electromagnetic parameters of the sample in the frequency band of 2–18 GHz, the sample was compressed to a cylindrical with 7.00 mm outer diameter, 3.04 mm inner diameter (60 wt% sample and 40 wt% paraffin) and measured by vector network analyzer (VNA).

3. Results and discussion

3.1 Schematic diagram of hollow core–shell ZnFe$_2$O$_4$@C nanospheres

Schematic diagram Fig. 1 depicts the preparation of the hollow core–shell ZnFe$_2$O$_4$@C nanospheres. Firstly, the hollow ZnFe$_2$O$_4$ nanospheres were synthesized by a solvothermal precipitation method and there are a lot of functional groups such as –COOH, –OH on their surface, which are conducive to the later growth of the PR shell. Secondly, the ZnFe$_2$O$_4$@PR nanospheres were calcined at a high temperature in the N$_2$ atmosphere, and the PR shell was carbonized into a dielectric C shell.

3.2 Morphology analysis

The surface morphology and internal microstructure of the as-prepared ZnFe$_2$O$_4$ and ZnFe$_2$O$_4$@C were characterized by SEM and TEM. Fig. 2(a) shows that pure ZnFe$_2$O$_4$ without a C shell is composed of heterogeneous nanospheres with an average size of 300–400 nm. It is noteworthy that some nanospheres in the figure show spherical rupture. Fig. 2(b) is a local magnified view of the fractured spheres. This rupture is most likely due to the impact of CO$_2$ and NH$_3$ gas produced during the formation of the hollow ZnFe$_2$O$_4$ spheres. Fig. 2(c) is a TEM image of ZnFe$_2$O$_4$. It can be seen from the figure that the sample dispersion well, and the spheres have different sizes, with an average size of 300–400 nm, which is following the SEM result. Interestingly, the color around the center of the nanosphere is slightly lighter than the outer ring of the nanospheres, which can be attributed to the formation of hollow ZnFe$_2$O$_4$. Fig. 2(d) is the SEM diagram after the introduction of the C shell. It can be clearly observed that the C shell is uniformly and completely coated on the ZnFe$_2$O$_4$ core, and the corresponding spherical size is also enlarged. Fig. 2(e) is a SEM local amplification of ZnFe$_2$O$_4$@C with core–shell structure. It can be observed from the figure that the C shell has a certain thickness, and this regular core–shell structure provides favorable conditions for the reflection and scattering of electromagnetic waves. Fig. 2(f) is TEM of ZnFe$_2$O$_4$@C, from which it can be observed that the chroma difference of ZnFe$_2$O$_4$ hollow structure is significantly weakened because the addition of C shell makes the size of spherical particles larger, which is not conducive to the observation of the inner cavity, but the hollow structure still exists. In addition, the presence of a C shell around the hollow ZnFe$_2$O$_4$ nanospheres was obviously observed, above all the pictures indicate that we have successfully prepared the hollow core–shell structure ZnFe$_2$O$_4$@C.

3.3 Structure analysis

The crystalline structure and phase composition of ZnFe$_2$O$_4$ and ZnFe$_2$O$_4$@C samples were characterized by X-ray diffractometer (XRD). As seen from Fig. 3, it can be observed that apparent diffraction peaks of ZnFe$_2$O$_4$, which are well consistent with the ZnFe$_2$O$_4$ (JCPDS card no. 22-1012),[22] the results indicate that ZnFe$_2$O$_4$ with good crystallinity has been successfully prepared. Compared with ZnFe$_2$O$_4$, the position of ZnFe$_2$O$_4$@C of the diffraction peak does not change except only the peak intensity decreases after recombination with the C shell. Another point worth noting is that there are no carbon peaks, which indicates that C exists in an amorphous state.[23]

The degree of graphitization of carbon in ZnFe$_2$O$_4$@C nanocomposite was investigated by Raman spectroscopy, and the result is shown in Fig. 4. There exist two obvious characteristic peaks of D and G bands at around 1350 cm^{-1} and
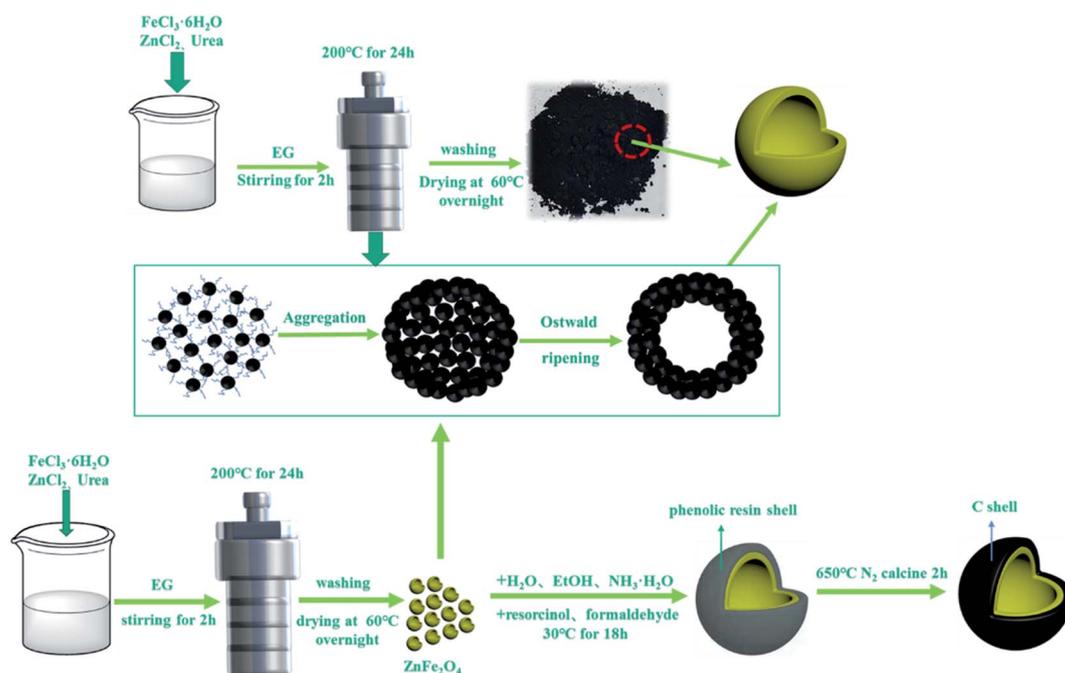

Fig. 1 Schematic illustration of the process for the synthesis of hollow core−shell ZnFe$_2$O$_4$@C composites.
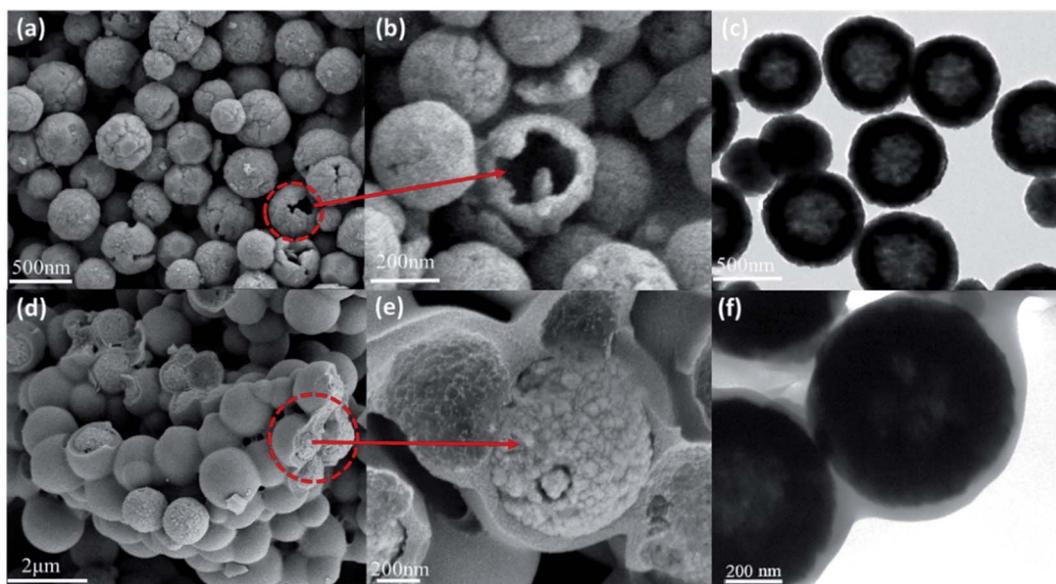
Fig. 2 SEM images of ZnFe$_2$O$_4$ (a and b) and ZnFe$_2$O$_4$@C (d and e); TEM images of ZnFe$_2$O$_4$ (c) and ZnFe$_2$O$_4$@C (f).
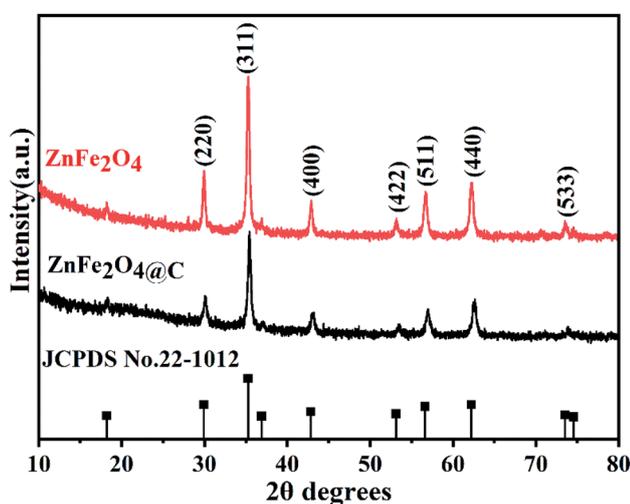
Fig. 3 XRD spectrum of ZnFe$_2$O$_4$ and ZnFe$_2$O$_4$@C composites.

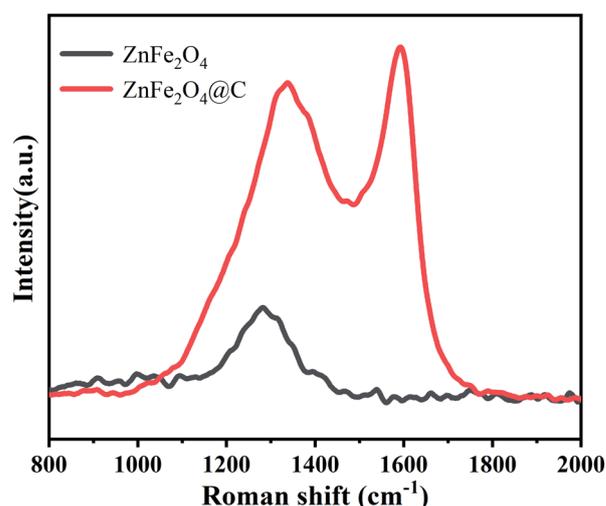**Fig. 4** The Raman patterns of ZnFe$_2$O$_4$@C composite.

1595 cm^{-1}. The peak of the D-band indicates the structural disorders and defects of the C shell,[24] while the peak of the G-band reveals the planar vibrations of graphite with lattice structure.[25] The intensity ratio of the D-peak to the G-peak (I_D/I_G) is usually used to describe the degree of disorder of carbon.[26] The I_D/I_G value of ZnFe$_2$O$_4$@C is relatively high (≈ 0.90), indicating that C shell has a certain degree of graphitization, so there are still many defects within the surface of C shell. The defects can be used as polarization centers to cause polarization relaxation, which contributes to the improvement of electromagnetic wave absorption.[27] These results are consistent with the results of XRD patterns and a previous report.[28]

The chemical composition and element valence states of the ZnFe$_2$O$_4$@C are further investigated by XPS. Fig. 5(a) shows the full spectrum of ZnFe$_2$O$_4$@C. Peaks at 284, 530, 721, and

1021 eV corresponded to C 1s, O 1s, Fe 2p, and Zn 2p orbitals, respectively. Fig. 5(b) presents that the Zn 2p spectrum can be deconvoluted into two peaks corresponding to Zn 2p$_{1/2}$ and 2p$_{3/2}$ at 1023.1 eV and 1044.5 eV, respectively, indicating that the Zn exists in a bivalent state, which is consistent with the existing form of Zn in spinel structure ZnFe$_2$O$_4$ reported in the previous literature.[29] Fig. 5(c) shows four binding energy peaks at 710.9 eV, 718.6 eV, 724.2 eV and 733.6 eV. Interestingly, the two peaks centered at 710.9 eV and 724.2 eV can be ascribed to Fe 2p$_{3/2}$ and Fe 2p$_{1/2}$, the other two peaks at 718.6 eV and 733.6 eV are consistent with reconstructed satellite peaks, which suggest Fe element is present as Fe^{3+} instead of Fe^{2+} in ZnFe$_2$O$_4$@C composite. In addition, the peak of Fe^{2+} was not shown, indicating that the prepared sample is pure and free of any impurities. The O 1s spectrum is displayed in Fig. 5(d) and the
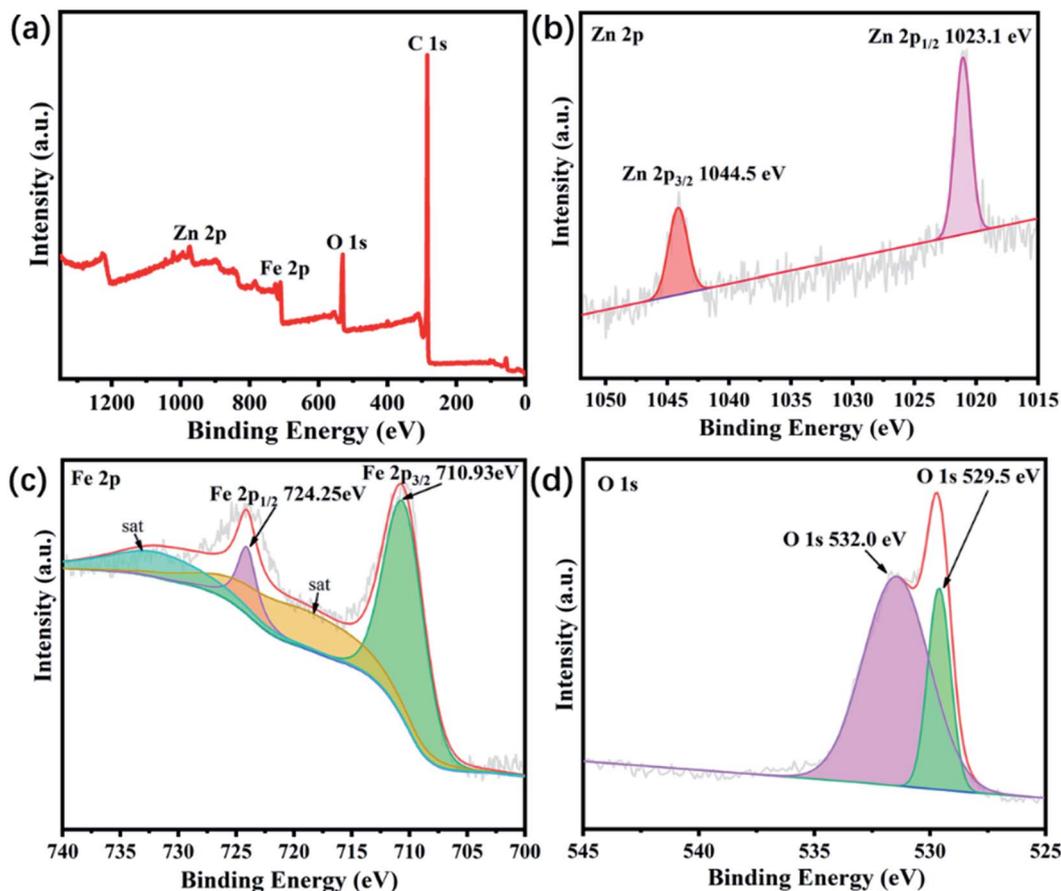
Fig. 5   XPS spectra of the $ZnFe_2O_4$@C composites: (a) full scan, (b) Zn 2p, (c) Fe 2p, (d) O 1s.

resolved peaks at 529.5 eV and 532.0 eV, the peak at 529.5 eV represents the lattice oxygen of Fe–O and Zn–O bonds in $ZnFe_2O_4$@C and the peak at 532.0 eV corresponds to –OH, H_2O and other substances adsorbed on the sample surface. This result, combined with XRD and Raman spectra, indicates that we have successfully prepared $ZnFe_2O_4$@C with good purity.

The hollow core–shell structure of the as-obtained $ZnFe_2O_4$@C was further investigated by the nitrogen adsorption and desorption test to characterize the specific surface area and pore size type and distribution. As revealed in Fig. 6, the adsorption–desorption isotherms curves all show a typical type IV isotherm, which indicates that all the samples exist in mesoporous structure.[30] The surface area of $ZnFe_2O_4$ and $ZnFe_2O_4$@C is 45.05 m^2 g^{-1} and 69.87 m^2 g^{-1}, which may be attributed to the introduction of dielectric C shell not only reducing the light-weight of the composite but also increasing the interfacial area.
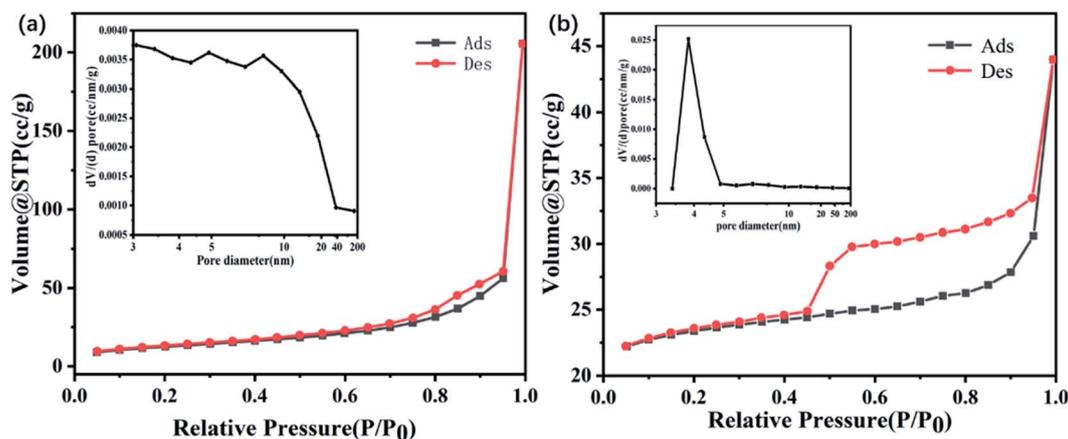

Fig. 6   Nitrogen adsorption–desorption isotherm and pore size distribution curves of $ZnFe_2O_4$ (a) and $ZnFe_2O_4$@C (b).
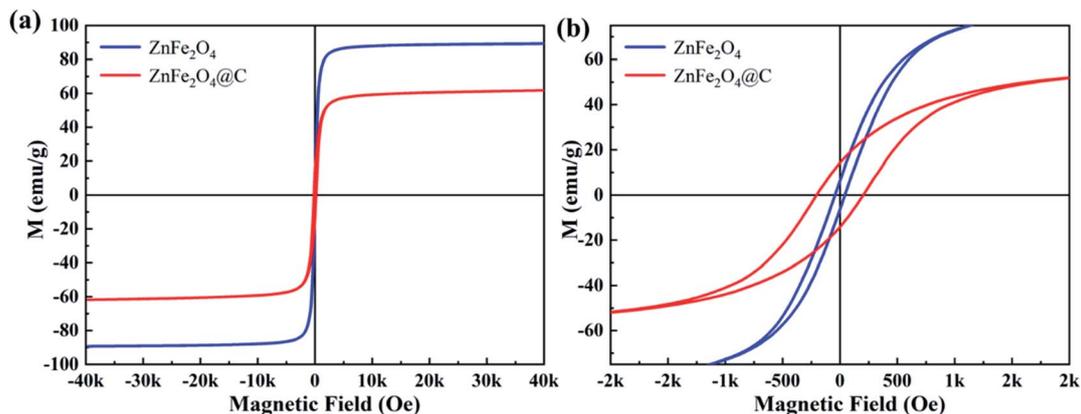
Fig. 7 Magnetic hysteresis loops for $ZnFe_2O_4$ and $ZnFe_2O_4$@C.

The illustrations of Fig. 6(a) and (b) show the pore size distribution of $ZnFe_2O_4$ and $ZnFe_2O_4$@C, respectively. The pore size distribution of $ZnFe_2O_4$ is relatively uneven, mainly distributed in 3–40 nm. The large pore size distribution may be due to the fracture of some $ZnFe_2O_4$ hollow structures. After the introduction of dielectric C shell, the pore size distribution is mainly distributed in 3–5 nm, and its pore size is significantly smaller, which may be because C shell is a complete and uniform coating on $ZnFe_2O_4$ core, filling the holes generated by the rupture of hollow $ZnFe_2O_4$. The large specific surface area and the presence of mesoporous pores are beneficial to the generation of interfacial polarization and the multiple reflection and refraction of electromagnetic waves.[31,32] Meanwhile, the $ZnFe_2O_4$@C of hollow core–shell structure is beneficial to the reduction of the density of the material, which provides favorable conditions for $ZnFe_2O_4$@C to become a lightweight microwave absorbing material.

3.4 Magnetic properties

The hysteresis loops of $ZnFe_2O_4$ and $ZnFe_2O_4$@C were measured by VSM at room temperature with a magnetic field between −40k and +40k Oe.

As shown in Fig. 7, all samples reach saturation at the magnetic field less than 10 kOe, which identify samples show typical soft magnetic properties, and the saturation magnetization (M_s) value of the $ZnFe_2O_4$ and $ZnFe_2O_4$@C was presented to be 89.25 emu g^{-1} and 61.82 emu g^{-1}, the remanent magnetization (M_r) were 6.39 emu g^{-1} and 14.19 emu g^{-1}, the coercivity was 50.17 Oe and 200.01 Oe, respectively. It's obvious that the M_s value of $ZnFe_2O_4$@C is evidently lower than the pure $ZnFe_2O_4$, which is caused by the dielectric C shell. The introduction of a dielectric C shell is beneficial to enhance the dielectric loss of the composite, which is conducive to the good impedance matching between dielectric loss and magnetic loss.[33]

3.5 Microwave absorption properties

The prepared core–shell structure is composed of $ZnFe_2O_4$ with magnetic loss and a C shell with dielectric loss. The complex

dielectric constant ($\varepsilon = \varepsilon' - j\varepsilon''$) and complex permeability ($\mu = \mu' - j\mu''$) of the core–shell structure $ZnFe_2O_4$@C are further studied at 2–18 GHz to investigate the microwave absorbing mechanism of the composite material by the vector network analyzer. The real and imaginary parts of the complex permittivity represent the storage and attenuation capacity of the sample to the electric energy, and the real and imaginary parts of the complex permeability represent the storage and loss capacity of the sample to the magnetic energy, respectively.[34] From Fig. 8(a), it can be vividly seen that the ε' values of $ZnFe_2O_4$ and $ZnFe_2O_4$@C present a roughly similar trend. Compared with $ZnFe_2O_4$@C, the real part of complex permittivity are higher than $ZnFe_2O_4$ at 2.0–10.2 GHz, the value varies from 7.5 to 8.5. With increasing frequency from 10.2 to 18.0 GHz, the real part of complex permittivity possesses a reverse trend. The imaginary part of the complex permittivity value of the $ZnFe_2O_4$ is lower than $ZnFe_2O_4$@C in the whole frequency, that's because the nonmagnetic C shell reduces the magnetism of $ZnFe_2O_4$@C. Meanwhile, the ε'' value curves of $ZnFe_2O_4$ and $ZnFe_2O_4$@C present a peak around 11.7 GHz, which can be accounted for the interfacial polarization of $ZnFe_2O_4$/air, $ZnFe_2O_4$/paraffin, $ZnFe_2O_4$/C, C/air. Besides, dielectric loss tangent ($\tan \delta\varepsilon = \varepsilon''/\varepsilon'$) are utilized to elucidate the dielectric dissipation performance of the microwave absorbers. It is evidently observed that the $\tan \delta\varepsilon$ of $ZnFe_2O_4$/C is higher than the $ZnFe_2O_4$ during the whole frequency range, which shows $ZnFe_2O_4$@C own much excellent dielectric loss property. μ' value of $ZnFe_2O_4$ and $ZnFe_2O_4$@C are display a monotonically decreasing trend, which decreases from 1.5 at 2.0 GHz to 0.9 at 18 GHz and 2.2 at 2.0 GHz to 0.8 at 18 GHz respectively. It's notable that the phenomenon is typical frequency dispersion behavior and is usually found in carbon-based microwave absorption material.[35] As shown in Fig. 8(e), the μ'' value presents a decreasing trend with moderate fluctuations, the value ranging from 0.68 to 0.05 and 0.5 to −0.02, respectively. The existence of the negative value of μ'' was interpreted to the partial eddy current loss caused by the movement of charge between C shell and $ZnFe_2O_4$. As seen in Fig. 8(f), the curves of $\tan \delta\mu$ of $ZnFe_2O_4$ and $ZnFe_2O_4$@C have highly similar changing trends, which certify there is no evident difference about the magnetic loss
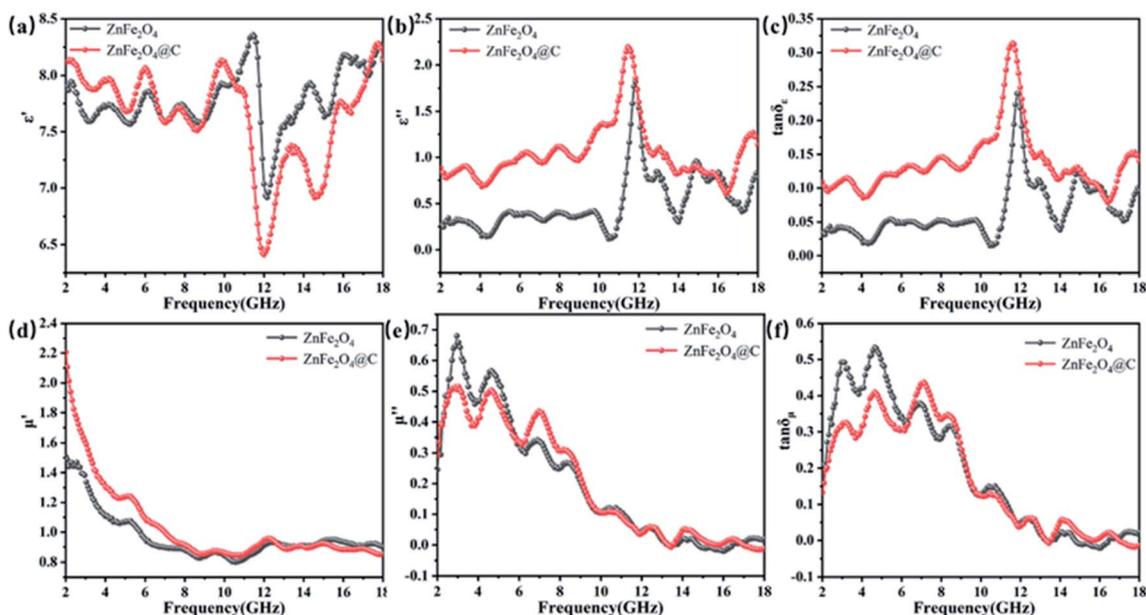
Fig. 8 (a) Real part of complex permittivity; (b) imaginary part of complex permittivity; (c) tangent of dielectric loss; (d) real part of complex permeability; (e) imaginary part of complex permeability; (f) tangent of magnetic loss.

mechanisms. It's notable that, the value of tan δε and tan δμ of ZnFe₂O₄, ZnFe₂O₄/C are close to each other, indicating that EM microwave absorption capability of ZnFe₂O₄, ZnFe₂O₄/C is the result of the synergistic effect of magnetic loss and dielectric loss.

To further evaluate the microwave absorption performance of ZnFe₂O₄ and ZnFe₂O₄@C, the reflection loss (RL) values are calculated by a vector network analyzer (VNA). In general, an RL value of less than −10 dB means that the microwave absorbing material can absorb 90% of the electromagnetic wave. Therefore, a material with an RL value of less than −10 dB is considered a suitable electromagnetic wave absorbing material. According to the transmission line theory, the RL$_{max}$ of the sample was calculated and analyzed by the following formula:
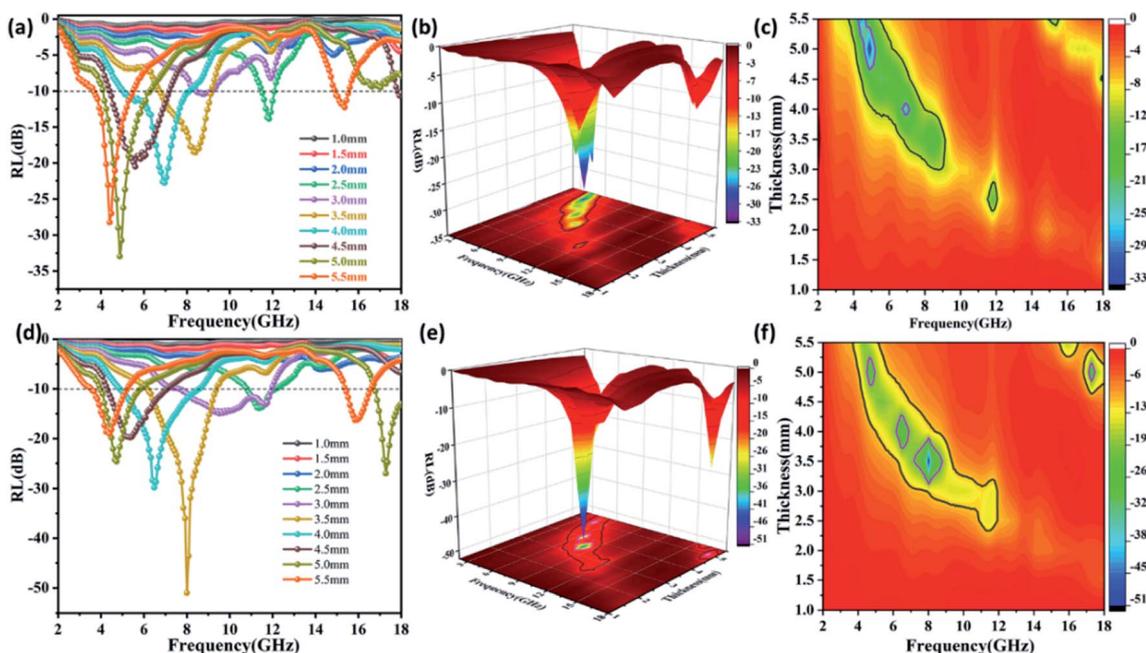

Fig. 9 Reflection loss curves of (a) ZnFe₂O₄, (d) ZnFe₂O₄@C, 3D RL curves of (b) ZnFe₂O₄, (e) ZnFe₂O₄@C, 2D projection curves of (c) ZnFe₂O₄, (f) ZnFe₂O₄@C.

$$\mathrm{RL(dB)} = 20 \log \left| \frac{Z_{\mathrm{in}} - Z_0}{Z_{\mathrm{in}} + Z_0} \right| \qquad (1)$$

The reflection loss of $ZnFe_2O_4$ and $ZnFe_2O_4@C$ are calculated and analyzed according to the formula (1). As depicted in Fig. 9, the RL_{max} of $ZnFe_2O_4$ reach -32.95 dB with the bandwidth of 2.24 GHz (4.08–6.32 GHz) and $ZnFe_2O_4@C$ reach -50.97 dB with the bandwidth of 3.2 GHz (6.16–9.36 GHz), meanwhile, it can be seen from the 2D projection curve that the projected area of $ZnFe_2O_4@C$ is always larger than single $ZnFe_2O_4$, no matter the reflection loss is less than -10 dB or -20 dB. Compared with a single $ZnFe_2O_4$, the optimal microwave absorbing performance of $ZnFe_2O_4@C$ is significantly increased, and the coating thickness of the sample decreases from 5.0 mm to 3.5 mm at the optimal reflection loss, which will be beneficial to the sample being widely used as a lightweight microwave absorbing material. Furthermore, the reflection loss of both samples moves to the low frequency with the increased coating thickness, which can be explained by the $\lambda/4$ matching model.[36]

The impedance matching (Z) refers to the degree of matching between the free space and the material, attenuation constant (α) is comprehensive electromagnetic wave attenuation ability capability, both of them are also two important factors to evaluate the microwave absorbing performance, which can be described as follows:

$$Z = \left| \frac{Z_{\mathrm{in}}}{Z_0} \right| = Z_0 \sqrt{\frac{\mu_{\mathrm{r}}}{\varepsilon_r}} \tanh \left(j \frac{2\pi f_{\mathrm{m}} d \sqrt{\varepsilon_{\mathrm{r}} \mu_{\mathrm{r}}}}{c} \right) \qquad (2)$$

$$\alpha = \frac{\sqrt{2}\pi f_{\mathrm{m}}}{c} \times \sqrt{\mu'' \varepsilon'' - \mu' \varepsilon' + \sqrt{(\mu'' \varepsilon'' - \mu' \varepsilon')^2 + (\mu' \varepsilon'' + \mu'' \varepsilon')^2}} \qquad (3)$$

Z_0 is impedance in free space, Z_{in} is impedance of microwave absorbing material, c is velocity of light, d is coating thickness of microwave absorbing material, f_{m} is frequency of electromagnetic wave.

It can be vividly seen from Fig. 10, the attenuation constant α is not gradually increasing with the increasing frequency, which may be due to the microwave absorbing material's owning different attenuation properties in different bands. It should be noticed that $ZnFe_2O_4@C$ have a higher value than $ZnFe_2O_4$ during the frequency range of 2.0–18 GHz, indicating $ZnFe_2O_4@C$ has more excellent electromagnetic wave attenuation performance, which has the largest α value is 110.52. Theoretically, the greater the value of α, the better the attenuation performance of the sample to the electromagnetic wave, but in fact, it is not so. Based on this, we further analyzed the relationship between the optimal reflection loss, impedance matching, Z, and attenuation coefficient α, as shown in Fig. 10.

Generally speaking, the closer Z value is to 1, the better impedance matching degree is, and the more electromagnetic waves can enter the material without being reflected off, which is conducive to the loss of electromagnetic waves in the material. We single select α, Z, RL curves of $ZnFe_2O_4$, Z value of $ZnFe_2O_4$ is equal to 1 at 4.32 GHz and 6.24 GHz at low
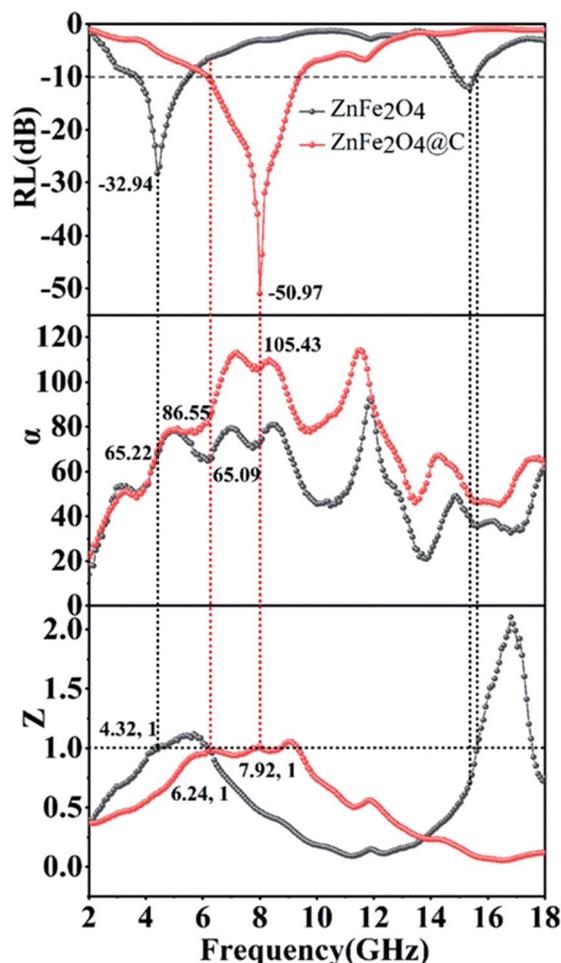

Fig. 10 The frequency dependence of RL values, attenuation constant (α) and impedance matching value (Z).

frequency, and the corresponding attenuation coefficient α value is 65.22 and 65.09, respectively. It is easy to conclude that when the Z value is 1, a larger α value has a larger reflection loss value. This phenomenon is not so regular in the high-frequency region, which indicates that the best reflection loss of the sample may be dominated by the attenuation coefficient α or the impedance matching Z value, or they determine the best reflection loss of the sample together. Similarly, the curves of $ZnFe_2O_4@C$ present the phenomenon, Z value is equal to 1 at 6.24 GHz and 7.92 GHz, and α value is 86.55 and 105.43. It's apparent that the RL corresponding to different α values is -10.58 dB and -50.97 dB, respectively. This result further proves that excellent microwave absorbing performance is the synergistic effect of attenuation coefficient α and impedance matching Z value.

The magnetic loss mechanism of microwave absorbing materials mainly includes natural resonance, exchange resonance, domain wall resonance, and eddy current loss.[37] However, domain wall resonance occurs mainly in the MHz range and is generally not considered. In the 2–18 GHz range, natural resonances generally occur at low frequencies and exchange resonances at high frequencies. The generation of
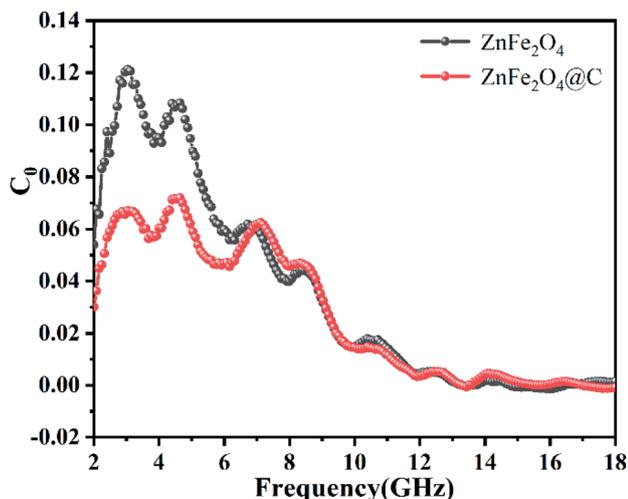
Fig. 11 C_0 values of ZnFe$_2$O$_4$ and ZnFe$_2$O$_4$@C.

eddy current effect is generally evaluated by the value of C_0, the equation is as formula (4), when the value of C_0 approaches a certain constant, eddy current losses play a major role. As shown in Fig. 11, when in the frequency range of 2–12 GHz, the C_0 values of ZnFe$_2$O$_4$ and ZnFe$_2$O$_4$@C vary greatly, which are the result of natural resonance. While, in the frequency range of 12–18 GHz, the C_0 value of ZnFe$_2$O$_4$ and ZnFe$_2$O$_4$@C fluctuate very small and tend to be constant, indicating that this frequency range is mainly determined by eddy current losses.

$$C_0 = \frac{\mu''}{\mu'^2 f_m} = 2\pi\mu_0 d^2 \sigma \qquad (4)$$

In order to investigate the electromagnetic wave loss mechanism, Fig. 12 shows the process of absorption and attenuation of electromagnetic waves. First of all, good impedance matching is very important for microwave absorbing performance.
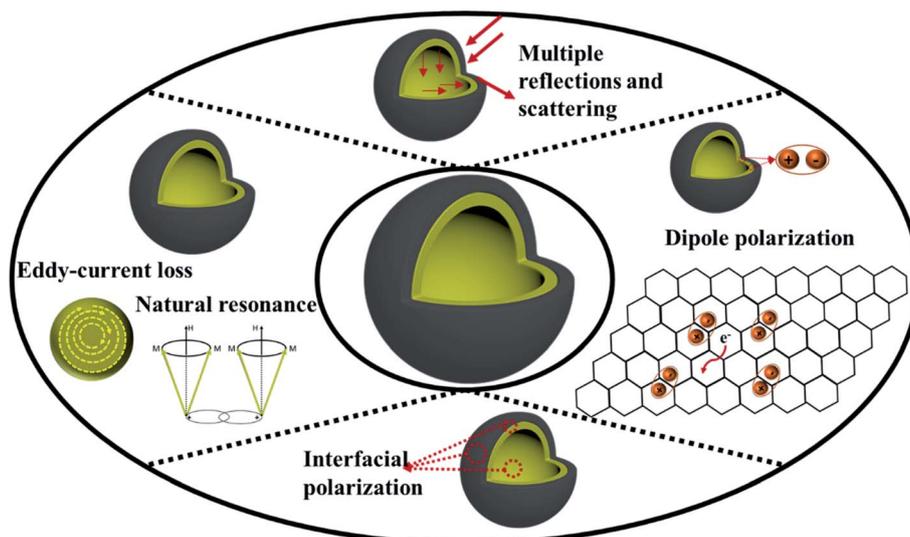
The magnetic properties of ZnFe$_2$O$_4$ and dielectric properties of C ensure the good impedance matching of ZnFe$_2$O$_4$@C material. The excellent impedance matching characteristics make the electromagnetic wave enter the material as much as possible without being reflected off, which provides a good condition for the loss of electromagnetic waves. Due to the special hollow core–shell structure of ZnFe$_2$O$_4$@C, the electromagnetic wave entering the material can be reflected and scattered many times in the internal cavity, and thus be lost and attenuated. Secondly, core–shell structure exists a lot of interfacial areas lead to the charge accumulation and vibration under the alternating magnetic field, which is beneficial to the more excellent interfacial polarization. Thirdly, the formation of C shell during the calcination process will produce a large number of defects, which also promote the formation of dipoles, conducive to the generation of dipole polarization, meanwhile, C shell exists in the form of conductive grid, which can be used as electron transmission channel to improve the conductivity of nanocomposites and facilitate the accumulation of charge at the interface, which is also facilitate to the generation of dipole polarization. Last but not least, ZnFe$_2$O$_4$ is the magnetic component of ZnFe$_2$O$_4$@C material, its unique magnetism makes ZnFe$_2$O$_4$@C produce natural resonance at low frequency and eddy current loss at high frequency, which also increases the ability to lose electromagnetic waves.

4. Conclusion

In this paper, a novel hollow core–shell ZnFe$_2$O$_4$@C microwave absorber had been successfully synthesized by *in situ* oxidation polymerization method. It was observed that introducing a dielectric C shell exerted an important influence on the microwave absorbing performance. The data indicated that the excellent reflection loss of the hollow core–shell ZnFe$_2$O$_4$@C composites reached −50.97 dB at 8.0 GHz with a thickness of 3.5 mm and the microwave absorption bandwidth with the

Fig. 12 Schematic illustration of the microwave absorption mechanism of hollow core–shell ZnFe$_2$O$_4$@C composite.

reflection loss under −10 dB was 3.2 GHz (6.16–9.36 GHz). It was concluded that the special hollow core–shell structure formed by introducing C shell and the microwave absorbing performance was obviously improved. This apparent improvement in microwave absorbing performance can be attributed to the special hollow core–shell structure and the synergistic effect of magnetic $ZnFe_2O_4$ with dielectric C shell, which played a vital role in the attenuation of electromagnetic waves. The preparation of $ZnFe_2O_4$@C with a special hollow core–shell structure provided a feasible idea for the preparation of lightweight and efficient microwave absorbing materials, which are expected to become a new type of microwave absorbing materials.

Funding

Ethical statement

This article has been approved by the institutional committee of Shanghai University of Engineering Science. All procedures performed in studies involving humans were in accordance with the ethical standards of the institution or practice at which the studies were conducted.

Consent to participate

All authors have agreed on the participation of submission.

Conflicts of interest

All authors certify that there is no conflict of interest in this study.

Acknowledgements

References

1 J. Liu, H. Zhang, R. Sun, et al. Hydrophobic, flexible, and lightweight mxene foams for high-performance electromagnetic-interference shielding, Adv. Mater., 2017, 29(38), 1702367.

2 X. Xie, B. Wang, Y. Wang, et al. Spinel structured MFe_2O_4 (M = Fe, Co, Ni, Mn, Zn) and their composites for microwave absorption: A review, Chem. Eng. J., 2022, 428, 131160.

3 D. Zhi, T. Li, J. Li, et al. A review of three-dimensional graphene-based aerogels: Synthesis, structure and application for microwave absorption, Composites, Part B, 2021, 211, 108642.

4 V. Sapna, N. Budhiraja, V. Kumar, et al. Shape-controlled synthesis of superparamagnetic $ZnFe_2O_4$ hierarchical structures and their comparative structural, optical and magnetic properties, Ceram. Int., 2019, 45(1), 1067–1076.

5 Z. Yang, Y. Wan, G. Xiong, et al. Facile synthesis of $ZnFe_2O_4$/reduced graphene oxide nanohybrids for enhanced microwave absorption properties, Mater. Res. Bull., 2015, 61, 292–297.

6 Y. Wang, X. Gao, X. Wu, et al. Hierarchical $ZnFe_2O_4$@RGO@CuS composite: Strong absorption and wide-frequency absorption properties, Ceram. Int., 2018, 44(8), 9816–9822.

7 G. Wu, H. Zhang, X. Luo, et al. Investigation and optimization of Fe/$ZnFe_2O_4$ as a wide-band electromagnetic absorber, J. Colloid Interface Sci., 2019, 536, 548–555.

8 X. Huang, Y. Qin, Y. Ma, et al. Preparation and electromagnetic properties of nanosized $ZnFe_2O_4$ with various shapes, Ceram. Int., 2019, 45(15), 18389–18397.

9 Y. Ge, Z. Wang, M. Yi, et al. Fabrication and magnetic transformation from paramagnetic to ferrimagnetic of $ZnFe_2O_4$ hollow spheres, Trans. Nonferrous Met. Soc. China, 2019, 29(7), 1503–1509.

10 B. Dai, J. Li, W. Wang, et al. Carbon fibers with eddy current loss characteristics exhibit different microwave absorption properties in different graphitization states, Mater. Lett., 2020, 281, 128667.

11 F. Sultanov, C. Daulbayev, B. Bakbolat, et al. Advances of 3D graphene and its composites in the field of microwave absorption, Adv. Colloid Interface Sci., 2020, 285, 102281.

12 C. Zhou, S. Geng, X. Xu, et al. Lightweight hollow carbon nanospheres with tunable sizes towards enhancement in microwave absorption, Carbon, 2016, 108, 234–241.

13 Y. Wang, W. Sun, K. Dai, et al. Flexible and heat-resistant carbon nanotube/graphene/polyimide foam for broadband microwave absorption, Compos. Sci. Technol., 2021, 212, 108848.

14 Y. Wang, W. Zhou, G. Zeng, et al. Rational design of multi-shell hollow carbon submicrospheres for high-performance microwave absorbers, Carbon, 2021, 175, 233–242.

15 X. Deng, S. Gao, J. Yan, et al. The green synthesis and enhanced microwave absorption performance of core–shell structured multicomponent alloy/carbon nanocomposites derived from the metal-sericin complexation, J. Alloys Compd., 2021, 882, 160680.

16 Y. Gu, P. Dai, W. Zhang, et al. Fe_3O_4 nanoparticles anchored on hierarchical porous carbon derived from egg white for efficient microwave absorption performance, Mater. Lett., 2021, 304, 130624.

17 W. Ma, P. He, T. Wang, et al. Microwave absorption of carbonization temperature-dependent uniform yolk–shell H-Fe_3O_4@C microspheres, Chem. Eng. J., 2021, 420(1), 129875.

18 J. Tao, J. Zhou, Z. Yao, et al. Multi-shell hollow porous carbon nanoparticles with excellent microwave absorption properties, Carbon, 2021, 172, 542–555.

19 H. Jia, H. Xing, X. Ji, *et al.* Self-template and *in situ* polymerization strategy to lightweight hollow MnO$_2$@polyaniline core–shell heterojunction with excellent microwave absorption properties, *Appl. Surf. Sci.*, 2021, **537**, 147857.

20 X. Zhao, Y. Huang, X. Liu, *et al.* Core–shell CoFe$_2$O$_4$@C nanoparticles coupled with rGO for strong wideband microwave absorption, *J. Colloid Interface Sci.*, 2022, **607**(1), 192–202.

21 B. Wang, H. Chen, S. Wang, *et al.* Construction of core–shell structured Co$_7$Fe$_3$@C nanocapsules with strong wideband microwave absorption at ultra-thin thickness, *Carbon*, 2021, **184**, 223–231.

22 F. Li, W. Zhan, L. Zhuang, *et al.* Acquirement of strong microwave absorption of Znfe$_2$O$_4$@SiO$_2$@reduced graphene oxide/pvdf composite membranes by regulating crystallization behavior, *J. Phys. Chem. C*, 2020, **124**(27), 14861–14872.

23 B. Han, W. Chu, X. Han, *et al.* Dual functions of glucose induced composition-controllable Co/C microspheres as high-performance microwave absorbing materials, *Carbon*, 2020, **168**, 404–414.

24 R. Shu, Y. Wu, W. Li, *et al.* Fabrication of ferroferric oxide–carbon/reduced graphene oxide nanocomposites derived from Fe-based metal–organic frameworks for microwave absorption, *Compos. Sci. Technol.*, 2020, **196**, 108240.

25 A. C. Ferrari, S. E. Rodil and J. Robertson, Interpretation of infrared and Raman spectra of amorphous carbon nitrides, *Phys. Rev. B: Condens. Matter Mater. Phys.*, 2003, **67**(15), 1553061–15530620.

26 D. Liu, R. Qiang, Y. Du, *et al.* Prussian blue analogues derived magnetic FeCo alloy/carbon composites with tunable chemical composition and enhanced microwave absorption, *J. Colloid Interface Sci.*, 2018, **514**, 10–20.

27 Z. Sun, Z. Yan, K. Yue, *et al.* Multi-scale structural nitrogen-doped rGO@CNTs composites with ultra-low loading towards microwave absorption, *Appl. Surf. Sci.*, 2021, **538**, 147943.

28 E. Yang, X. Qi, R. Xie, *et al.* Core@shell@shell structured carbon-based magnetic ternary nanohybrids: Synthesis and their enhanced microwave absorption properties, *Appl. Surf. Sci.*, 2018, **441**, 780–790.

29 H. Li, Y. Hou and L. Li, Tunable design of yolk–shell ZnFe$_2$O$_4$@C composites for enhancing electromagnetic wave absorption, *Powder Technol.*, 2021, **378**, 216–226.

30 Y. Du, T. Liu, B. Yu, *et al.* The electromagnetic properties and microwave absorption of mesoporous carbon, *Mater. Chem. Phys.*, 2012, **135**(2), 884–891.

31 W. Bo, C. Zhou, Z. Yao, *et al.* Encapsulation of high specific surface area red blood cell-like mesoporous carbon spheres by magnetic nanoparticles: A new strategy to realize multiple electromagnetic wave loss mechanism, *Carbon*, 2021, **184**, 232–244.

32 Y. Cheng, Z. Li, Y. Li, *et al.* Rationally regulating complex dielectric parameters of mesoporous carbon hollow spheres to carry out efficient microwave absorption, *Carbon*, 2018, **127**, 643–652.

33 D. Zhang, Y. Xiong, J. Cheng, *et al.* Synergetic dielectric loss and magnetic loss towards superior microwave absorption through hybridization of few-layer WS$_2$ nanosheets with NiO nanoparticles, *Sci. Bull.*, 2020, **65**(2), 138–146.

34 R. Deng, B. Chen, H. Li, *et al.* MXene/Co$_3$O$_4$ composite material: Stable synthesis and its enhanced broadband microwave absorption, *Appl. Surf. Sci.*, 2019, **488**, 921–930.

35 S. Wang, H. Ren, W. Lian, *et al.* Dispersed spherical shell-shaped palygorskite/carbon/polyaniline composites with advanced microwave absorption performances, *Powder Technol.*, 2021, **387**, 277–286.

36 R. Shu, G. Zhang, X. Wang, *et al.* Fabrication of 3D net-like MWCNTs/ZnFe$_2$O$_4$ hybrid composites as high-performance electromagnetic wave absorbers, *Chem. Eng. J.*, 2018, **337**, 242–255.

37 Z. Liao, M. Ma, Z. Tong, *et al.* Fabrication of ZnFe$_2$O$_4$/C@PPy composites with efficient electromagnetic wave absorption properties, *J. Colloid Interface Sci.*, 2021, **602**, 602–611.